

Mathematical model to evaluate the ohmic resistance caused by the presence of a large number of bubbles in Hall-Héroult cells

A.L. PERRON, L.I. KISS* and S. PONCSÁK

Département des sciences appliquées, Université du Québec à Chicoutimi, Québec, Canada G7H 2B1

*(*author for correspondence, tel.: +1-418-545-5011, fax: +1-418-545-5018, e-mail: lkiss@uqac.ca)*

Received 21 2 2006; accepted in revised form 15 8 2006

Key words: alumina reduction cell, gas bubbles, interelectrode resistance, mathematical model

Abstract

Bubbles play an important role in the productivity of an electrolysis cell. They induce flow in the cell and increase the overvoltage, which is still two times greater than the thermodynamic voltage. Their contribution to the total electrical resistance of the electrolyte must be known for several reasons such as the energy efficiency and control. A computationally efficient mathematical model has been proposed that computes the total resistance of the electrolyte by using the concept of parallel-connected current tubes. The resistance of the individual current tubes has been determined earlier by the solution of the Laplace equation around the bubbles by the finite element method. Both electrical resistance models take into account the morphology (position, size and shape of each bubble) of the bubble layer. The current-tube model has been compared to the solutions obtained by a finite element method (FEM) for several real and hypothetical situations, using a large number of bubbles. The agreement between the results obtained by the proposed model and the FEM is very good. The difference between the two approaches is around 5% for a covering factor of 50%.

List of symbols

A_0	unperturbed area (m ²)
A_a	anode area (m ²)
A_t	total projected area (m ²)
A_p	total perturbed area (m ²)
b	bubble resistance factor
h	thickness of the bubble layer (m)
c	relative size of the perturbed zone
d_B	bubble diameter (m)
d	diameter (m)
L_{ACD}	anode–cathode distance (m)
$N(j)$	number of bubbles at time step j
R	electrical resistance (Ω)
V_B	bubble volume (m ³)

Greek symbols

κ	electrical conductivity (Ω ⁻¹ m ⁻¹)
ε	volume fraction of gas or void fraction
Θ	covering factor

Subscripts

0	bubble free-electrolyte
n	index of a bubble
T	electrolyte with the presence of the bubbles

Superscript

*	electrical current tube
j	time step

1. Introduction

In the Hall-Héroult process, the anode and the cathode are arranged horizontally, as shown in Figure 1 [1]. The liquid aluminium is produced by the reduction of alumina dissolved in an electrolyte mainly containing cryolite at 960 °C. The aluminium is deposited at the cathode and bubbles are generated

under the carbon anode. The density of the cryolite (bath) is slightly lower than that of the liquid aluminium. Being immiscible, the two liquid phases are separated physically by an interface. The bubbles are produced at preferential sites called “nucleation sites”. When the bubbles reach a critical volume, they start to move and they escape from the anode bottom. Along the vertical sidewall (sidewall channel), the

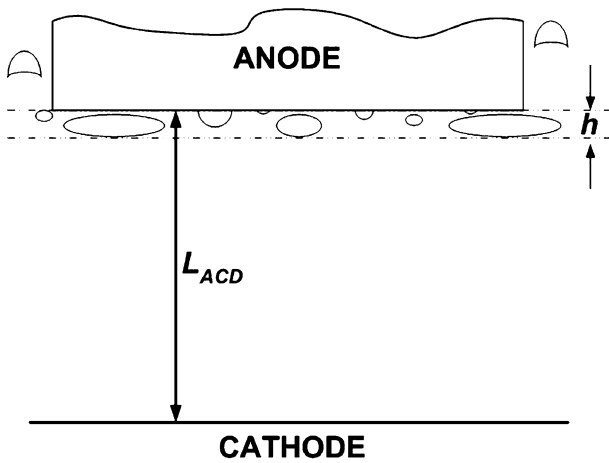


Fig. 1. Classical representation of the inter-electrode zone to compute the total resistance of the electrolyte.

bubble rises vertically until it escapes via the air-bath interface.

The presence of the bubbles plays a significant role in the efficiency of the Hall-Héroult cell. Their presence has positive and negative impacts. The flow induced by the bubbles transports the alumina to the reaction sites but it also creates instabilities at the bath-metal interface causing its deformation. Vertical flow components must be avoided at the interface because the density difference between the cryolite and the molten aluminium is small. The movement of bubbles increases the turbulence intensity which improves the mixing and the dissolution rate of the alumina in the bath. The quasi-horizontal flow under the anode promotes a heat flux directed to the sidewall to homogenize the temperature field. This horizontal heat flux plays a critical role in maintaining the protecting sidewall freeze. The most important negative effect on the energy balance of the cell is certainly their contribution to the overvoltage of the cell. Indeed, their impact is not negligible being 0.15 to 0.35 V [2]. They hinder the passage of current by reducing the conducting area and they deform the electrical field in the bubble-free zone located under the two-phase layer. Furthermore, the knowledge of the contribution of the bubbles to the increment of electrical resistance is a crucial parameter to evaluate the value of the anode-cathode distance L_{ACD} under normal operating conditions. Several theoretical works [3–6] have been devoted to the development of correlations predicting the role of the bubbles on the electrical resistance of the electrolyte. In the next section it will be shown that these expressions are based on morphological parameters of the bubble layer which are more often estimated than measured. These correlations do not take into account the size distribution of the bubbles and the interaction between them as well as the dynamic nature of the bubble layer. A lot of work has also been reported on laboratory experiments [7–12]. Although these small-scale electrochemical

models are very useful to study the role of the small bubbles, their anode sizes are generally too small to represent the real size distribution and the fluctuating behaviour of bubbles.

The classical hypothesis to evaluate the contribution of the bubbles on the effective resistance of the electrolyte is to separate it in two parts such as the bubble layer zone (BLZ) of thickness h and the bubble-free zone (BFZ) of thickness $L_{ACD} - h$ as shown in Figure 1. In this situation, the total resistance R_T of the bath is simply given by

$$R_T = R_{BFZ} + R_{BLZ} = \frac{(L_{ACD} - h)}{\kappa_0 A_a} + \frac{h}{\kappa_B A_a} \quad (1)$$

where A_a is the conducting surface (anode area), κ_0 and κ_B are the electrical conductivity in the bubble-free zone and in the bubble layer respectively. The relative electrical resistance may be obtained by dividing Equation 1 by the resistance of the electrolyte R_0 in the absence of bubbles

$$\frac{R_T}{R_0} = \frac{h}{L_{ACD}} \left(\frac{\kappa_0}{\kappa_B} - 1 \right) + 1 \quad (2)$$

There are several relations to relate the equivalent conductivities κ_B and the conductivity of the continuous phase κ_0 such as the one from Bruggeman [13],

$$\frac{\kappa_0}{\kappa_B} = (1 - \varepsilon)^{-3/2} \quad (3)$$

where ε is the volume fraction occupied by the gas phase. Although the relation (3) has been developed for objects uniformly distributed and it is valid only for relatively small void fraction, numerous correlations have been based on the Bruggeman equation [3, 4, 12]. By inserting Equation 3 in 2, a general form of the classical model is obtained

$$\frac{R_T}{R_0} = \frac{h}{L_{ACD}} \left((1 - \varepsilon)^{-3/2} - 1 \right) + 1. \quad (4)$$

The alternative forms of Equation 4 obtained by the various authors are generally due to different expressions for the void fraction.

Correlations for the additional electrical resistance due to the presence of bubbles under the anode have also been based on laboratory experiments. Hyde and Welch [8] studied the effects of the accumulated gas volume under the anode, the anode-cathode distance L_{ACD} and the bubble shape on the total resistance. The bubbles were simulated by ceramic objects of known volume and shape inserted in a laboratory electrolysis cell producing lead. The electrical resistance of the electrolyte with and without bubbles was obtained by measuring the voltage drop of the cell with a high sampling rate, when the current was suddenly stopped. The results showed that the bubble resistance primarily depends on bubble volume and the effect of bubble shape is small. Thus, by considering all the bubbles as an equivalent cylinder with a diameter equal to the depth of

the bubble layer, they proposed the following relation for the relative resistance

$$\frac{R_T}{R_0} = \frac{1}{L_{ACD}} \left[(L_{ACD} - h) + \frac{h}{1 - \Theta} \right]. \quad (5)$$

where Θ is the covering factor defined by

$$\Theta = \frac{A_t}{A_a} \quad (6)$$

where A_t is the total projected bubble area on the anode surface A_a . Aaberg et al. [9] investigated the characteristics of the bubble layer under an anode in a small scale electrolysis cell. The anode diameter was less than 10 cm. By measuring simultaneously the volume of accumulated gas and the electrical resistance of the electrolyte, they deduced the covering factor and the thickness of the bubble layer with Equation 5. The volume of gas was obtained by measuring the rise of the electrolyte level as done by Solheim and Thonstad [4]. The typical covering factor was about 0.45. The thickness of the bubble layer varied from 0.4 to 0.6 mm. Quian et al. [10] developed an interesting electrochemical method to measure the resistance of the electrolyte in the presence of bubbles underneath the anode. The utilization of an ac voltage superimposed source permitted to isolate the bubble resistance. They compared their results with available data for vertical electrodes. Their error was less than 4%. Quian et al. [11] investigated the incremental resistance caused by the presence of the bubbles produced by an air-water model and by a water electrolysis cell with their above mentioned electrochemical method. At a given current density, the electrical resistance caused by the bubbles in the electrolysis cell was always greater than for the air-water model. The difference was about 20%. The authors attributed this discrepancy to the mechanism of bubble production. The size of the bubbles produced by the air-water model was bigger than that generated in the electrolysis cell. They concluded that water models are not adequate to model bubbles generated by electrolysis.

Zoric and Solheim [5] were the first to introduce the deformation of the electric current field in the entire anode-cathode zone caused by the presence of bubbles under the anode. They studied the anodic and cathodic current distribution perturbed by the presence of bubbles. The anodic current density reached local maxima close to the bubble. The cathodic current density had local minima depending on the position of the large bubbles. They also presented some correlations for the incremental voltage drop applicable in certain conditions. Thonstad et al. [6] developed an expression which contains perturbations generated by the presence of bubbles, such as the so called screening effect and the deformation of the electrical field in the bubble-free zone under the bubble layer

$$\frac{R_T}{R_0} = 1 + \left(\frac{1}{1 - \Theta} - 1 \right) \left(\frac{h}{L_{ACD}} + \frac{1 - \frac{h}{L_{ACD}}}{1 + 5\sqrt{\Theta} \frac{2(L_{ACD}-h)}{d_b}} \right) \quad (7)$$

where d_b is the bubble diameter of the large bubble. The numerical calculations showed that for a bubble with a radius of 100 to 150 mm at a covering factor of about 50%, the incremental voltage drop due to the presence of the bubbles could be 30% larger than that calculated by the classical models.

In this paper, a mathematical model is developed to compute the total electrical resistance caused by the presence of bubbles under the anode from the outputs of the bubble layer simulator developed by Kiss et al. [14–16]. In other words, the model described in this paper links the morphology of the bubble layer to the electrolyte resistance. The term ‘total resistance’ or ‘bubble resistance’ refers to the electrical resistance of the electrolyte in the entire interelectrode spacing when bubbles are present.

2. The bubble layer simulator

There exist several methods to compute the flow in the electrolyte induced by the bubbles. The CFD (computational fluid dynamic) methods have been used in many works [17–19]. The geometry of the cell suggests the use of a two-fluid flow model. Although several works have been reported with the Euler–Lagrange sub-model [17–19], the validity of the utilisation of this sub-model is questionable because the presence of a high volume fraction of gas under the anode and the presence of large non-spherical bubbles [20]. The use of the Euler–Euler model to simulate the electrolyte flow is more suitable [21]. In this sub-model, each phase (gas and liquid) has its own set of conservation equations (continuity, momentum, energy) and the interactions between phases are characterized by the jump conditions at the interfaces. Turbulence models are used in each phase. Velocity, temperature and species distributions as well as the turbulence intensity in the electrolyte flow are given by the Euler–Euler model. However, the space average used to solve the equation system removes the bubble identity and replaces it by a volume fraction of gas. The principal difficulty to compute the total resistance of the electrolyte from CFD calculations is how to link the void fraction to the covering factor. In other words, the morphology of the bubble layer is not known. Kiss et al. [14–16] have developed a Lagrangian bubble layer simulator. The model follows each bubble from its nucleation to its escape via the free surface located at the top of the sidewall channel. It allows for the interactions between bubbles such as coalescence. At each time step, the interactions between the phases are computed by solving the momentum balance equations. Although some simplifications have been done such as the use of a unique velocity of the electrolyte in the bubble layer and no turbulence model is used, the simulator gives very good results compared to industrial data [15, 16]. Using this approach, the morphology, i.e. the position, size, and shape of the bubbles in the

two-phase layer is computed at each time step. In other words, the size distribution as well as the variations of the volume fraction and the local value of the covering factor along the anode surface are known at each time step. For the moving bubbles, the simulator uses only the rounded disc bubble shape. A recent study [22] has investigated the influence of the bubble shape on the incremental electrical resistance due to the presence of a gas volume under the anode. The shapes of the bubbles during their evolution were divided into four classes. These classes were approximated by simple geometries like the *circular disc*, the *rounded disc*, the *truncated cylinder* and the so-called Fortin bubbles [23]. The results have shown that the use of the *circular disc* shape instead of the three other shapes introduces an error less than 5%. Furthermore, the error of neglecting the presence of the wetting film located between the bubble and the solid surface is less than 2%. Thus, an electrical model to compute the bubble resistance is developed from the morphological outputs given by the bubble layer simulator at each time step.

3. Mathematical model for the bubble resistance

First, to evaluate the electrical resistance of the electrolyte with the bubbles, the interelectrode space is decomposed into a multitude of vertical parallel current tubes containing a bubble of a diameter d_b at the center of their section of origin. A channel is shown in Figure 2. In this paper, i.e. in the proposed mathematical model as well as in the finite element method (FEM), the bubble shape used is the *circular disc* to ease the computational work. In this case, the bubble volume is simply given by $\pi d_b^2 h/4$, where $h = 0.5$ cm. The vertical dimension h of a large bubble under a solid surface is limited by the capillary forces and can be calculated as a function of the material properties. The diameter of these tubes d^* equals the diameter of the perturbed zone caused by the presence of the bubbles in the electrical field. For a bubble-free electrolyte, the current lines are vertical if

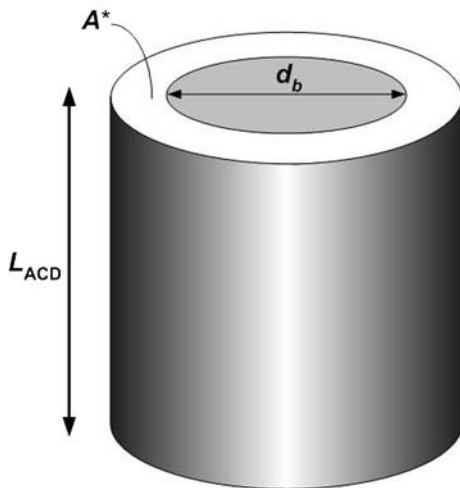


Fig. 2. An electrical current tube of cross-section A^* .

the medium is assumed isotropic. Since the bubbles deform these lines, a horizontal component of the electrical field is created. In this study, the limits of the perturbed zone were defined where the horizontal component equals 2% of the nominal current density. The relative size c_n of the zone perturbed by the bubble n is defined as

$$c_n = \frac{d_n^*}{d_{b,n}} \quad (8)$$

where d_n^* is the diameter of the perturbed zone. Then, the cross-section of the channel associated with the bubble n is given by

$$A_n^* = \frac{\pi}{4} (c d_b)_n^2 \quad (9)$$

Second, the bubble resistance increase factor b_n caused by the presence of the bubble n through its channel is

$$b_n = \left(\frac{R_T^*}{R_0^*} \right)_n \quad (10)$$

where R_0^* is the resistance of the current tube without bubble. The values of these two unknowns (c_n and b_n) are shown in Figure 3 as function of the bubble diameter. These values were computed using a finite element code described in a recent work [22]. To obtain good accuracy, mesh control has been used in the perturbed area. The coefficients c_n and b_n as function of the bubble diameter are given with a very good agreement ($R^2 \geq 0.995$) by the equations below

$$c_n = 5.3518 (d_b)_n^{-0.2634} \quad (11)$$

and

$$b_n = 0.9797 e^{0.0026^* d_{b,n}} \quad (12)$$

where d_b is expressed in mm. Then the total resistance for the channel n is given by

$$R_{T,n}^* = b_n R_{0,n}^* = 4b_n \left(\frac{L_{ACD}}{\kappa_0 \pi (c d_b)_n^2} \right). \quad (13)$$

The area A_0^j at the instant j is defined by

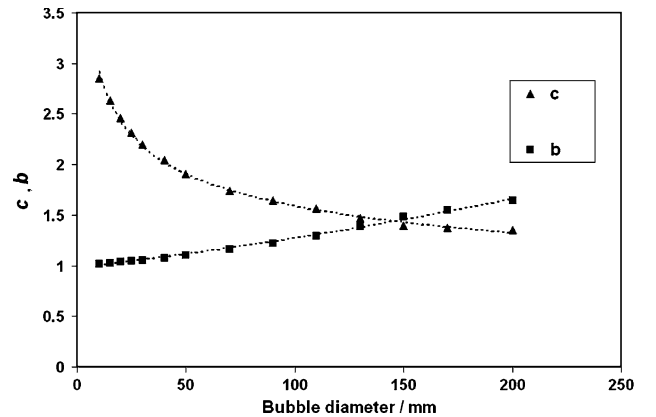


Fig. 3. Values of the coefficients c_n and b_n as function of the bubble diameter.

$$A_0^j = A_a - A_p^j = A_a - \sum_{n=1}^{N(j)} \left(\frac{\pi}{4} (c d_b)_n^2 \right) \quad (14)$$

where A_a is the anode area, A_p^j is the total perturbed zone and $N(j)$ is the number of bubbles. At low values of covering factor, A_0^j is positive. By summing the conductances of all the parallel current tubes containing bubble and the conductance of the bubble free-zone electrolyte, the total resistance of the interelectrode zone at the time step j is given by

$$R_T^j = \frac{1}{\frac{\kappa_0 A_0^j}{L_{ACD}} + \sum_{n=1}^{N(j)} \left(\frac{\pi \kappa_0 (c d_b)_n^2}{4 b_n L_{ACD}} \right)} \quad (15)$$

Equation 15 may be rewritten in a relative form by dividing each side by R_0

$$\frac{R_T^j}{R_0} = \frac{A_a}{A_0^j + \sum_{n=1}^{N(j)} \left(\frac{\pi (c d_b)_n^2}{4 b_n} \right)} \quad (16)$$

The summation in the denominator in Equation 16 represents the contribution of the conducting channels associated with the individual bubbles to the total resistance of the electrolyte independently of the anode size. The term A_0^j takes into account the size of the anode. At a covering factor lower than $\sim 35\%$, the anode area is greater than the perturbed zone A_p^j . However, at high covering factor, the perturbed zone calculated this way may be greater than the anode area. This virtual excess conducting section is principally caused by the overlapping of bubble channels and by the protrusion from under the anode. Its size depends on the bubble size distribution, on the number and the position of bubbles. This virtual excess conducting section – given also by the Equation 14 – must be removed from the total perturbed area in order to compute the relative resistance with the correct anode area. This subtraction is allowed since – as will be shown in the next section – the overlapping of the current channels does not induce additional resistance until a certain threshold distance between the bubbles is reached. Thus, Equation 16 is used to compute the relative resistance of the electrolyte for all values of the covering factor.

In this section, a mathematical model to evaluate the total resistance of the electrolyte has been developed. The model considers a multitude of cylindrical vertical current channels connected in parallel. In the following section, the model is tested for several spatial configurations of bubbles.

4. Validation, results and discussion

To validate the mathematical model described by Equations 14 and 16, the results given by the proposed

model have been compared to the solutions given by a finite element method FEM described in detail in a previous paper [22]. The 3D domain within which the Laplace equation is solved is identical to the previous one. It is composed principally of two parts; the anode and the electrolyte (cryolite). The ACD was kept constant at 5 cm for all the cases. The top of the anode and the bath-metal interface were assumed equipotential. Then, only the primary current distribution was calculated. The bubbles were simply represented by cavities. The limits of the domain as well as the bubble interface were considered to be insulating surfaces. In a first series of tests, the effects of overlapping have been investigated for a few bubbles of different diameters. Second, the model has been tested with a large number of bubbles of different sizes positioned randomly under a full scale anode ($50 \times 100 \text{ cm}^2$).

Figure 4 shows the relative resistance caused by the presence of one bubble, as a function of the bubble diameter. To avoid edge effects, the covering factor was kept constant for each diameter at 10%. Except at low diameters, the relative resistance calculated from the model is slightly higher than that obtained by the FEM. It is caused by the fact that the edge of the perturbed zone is defined at 2% deviation. The maximal resistance difference between the results given by the two approaches is 0.3% for the case of a single bubble. Figure 5 shows the different geometries used for the doublet, triplet and the quadruplet of bubbles. The dashed line around each bubble represents its perturbed zone. To study the effect of the overlapping of the perturbed zones on the electrical resistance, the distance between the bubbles is decreased successively until they touch each other. For each series of tests, the size of the bubbles is kept constant and the system is kept symmetrical, i.e. the bubble centers form either an equilateral triangle or a square.

Since the behaviour of the relative resistance as function of the normalized distance is similar for the three situations, only the results for the doublet of bubbles are presented in Figure 6. The normalized

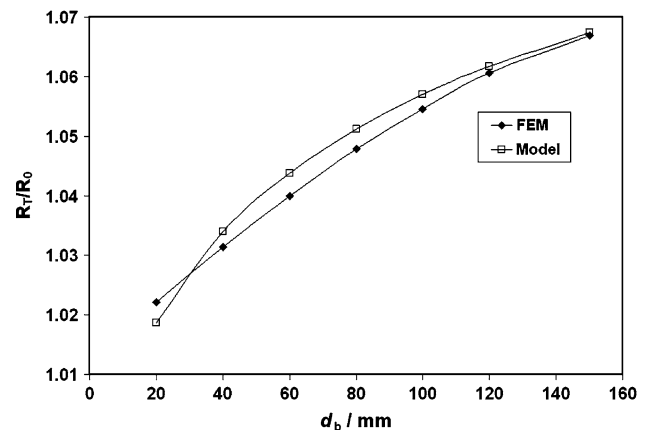


Fig. 4. Relative resistance calculated from the proposed model and from the FEM for a bubble.

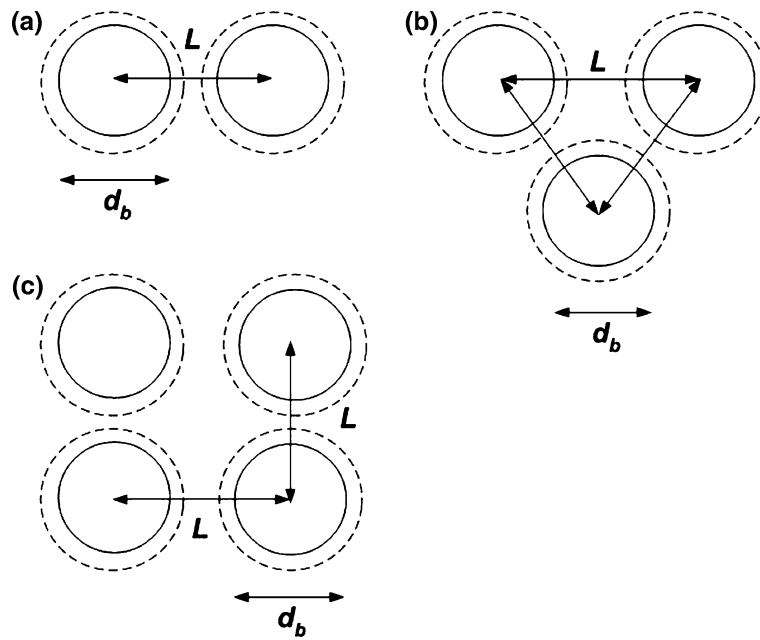


Fig. 5. Different configurations to study the overlapping between bubbles (bottom view): (a) doublet, (b) triplet, (c) quadruplet.

distance ND is simply defined by the ratio of the distance between the bubbles L to the bubble diameter d_b . The straight lines (without symbols) represent the results given by the model. Seven different bubble diameters are shown. At high ND, the bubbles are far away from each other thus their perturbed regions are not in contact. As the ND diminishes, the perturbed zones (described by the dashed line) overlap and the relative resistance remains constant until a certain distance. The constant value reflects the principle of superposition for solutions of a linear differential equation. For all simulations including the three configurations, the relative resistance begins to increase at around $L/d_b = 1.25$. At this distance, the bubbles are so close that they themselves overlap the perturbed zone of the other bubbles. This results in a slight increase of the relative resistance. Figure 7 shows the relative increase for the three different configurations at a

bubble diameter of 60 mm. The relative increase presented on the y -axis is defined as the ratio of the relative resistance when the bubbles touch each other to the case when the bubble channels do not overlap. It increases with the number of bubbles. The fact that a bubble is within a perturbed region of another bubble introduces a non-linearity in the domain of solutions. The model does not account of this effect. However, the discrepancy between both situations, i.e. at large and low ND, is less than 0.79% for a bubble diameter of 60 mm and it is less than 1% for the whole series of tests. Then, at low bubble number this effect is negligible. Although the model does not account for the preceding phenomenon, the difference in the relative resistance between the model and the FEM was less than 0.8% for the whole series of configurations studied.

The electrical model has also been tested in more complex situations with a higher number of bubbles as

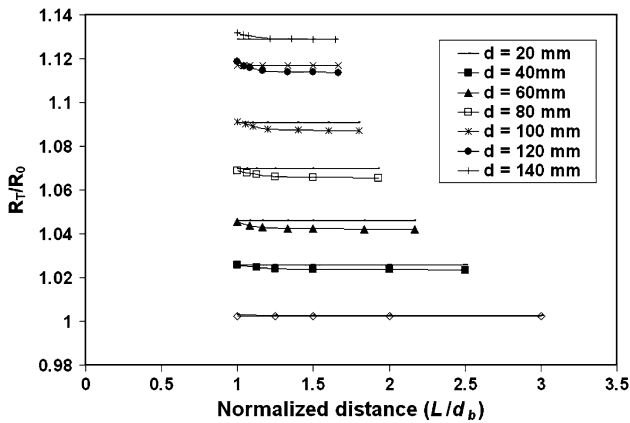


Fig. 6. Results obtained for the bubble doublet obtained from the proposed model and from the FEM.

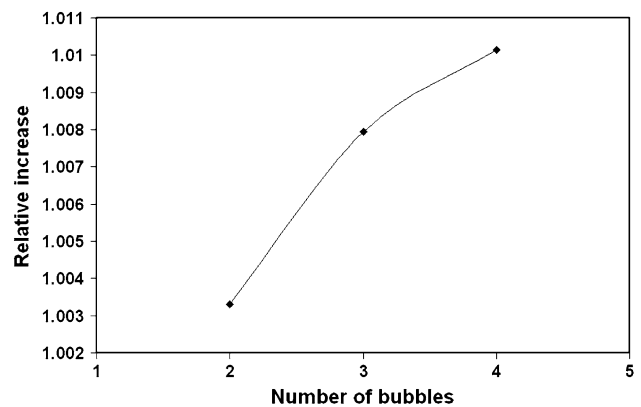


Fig. 7. Relative increase of the relative resistance as function of the number of bubbles for a bubble diameter of 60 mm.

well as with a higher covering factor. Figure 8 shows the relative difference between the values calculated from the present model and from the FEM

$$\begin{aligned} \text{difference} &= \left| \frac{\frac{R_T}{R_0}|_{\text{FEM}} - \frac{R_T}{R_0}|_{\text{model}}}{\frac{R_T}{R_0}|_{\text{FEM}}} \right| * 100 \\ &= \left| \frac{R_T|_{\text{FEM}} - R_T|_{\text{model}}}{R_T|_{\text{FEM}}} \right| * 100 \end{aligned} \quad (17)$$

as a function of the covering factor. The tests have been carried out on an anodic surface of $50 \times 100 \text{ cm}^2$. The number of bubbles was varied from 32 to 1566. The size distribution used in each test was random except at high bubble numbers, where the bubbles were as small as about 15 μm diameter. The maximal difference reaches 7% at a covering factor of 70%. The relation between this difference and the covering factor is not clear since the number of bubbles as well as the size distribution play a role. However, the difference seems to increase slightly with the covering factor. To verify if a correlation exists between the resistance difference and the number of bubbles, the results presented in Figure 8 are plotted against the number of bubbles in Figure 9.

The value of the difference seems to be independent of the number of bubbles. The average value of the difference between the results obtained by the two methods for all the studied cases is 2.7%. In order to investigate the deviation between the two approaches under normal operating conditions, several tests were done at a covering factor of around 50%. The results are presented in Figure 10. The average difference for cases where the number of bubbles exceeds 550 is 4.2%. The maximal difference of 7.3% is reached for 1566 bubbles.

It is important to mention that the differences expressed in this work are absolute values. At low covering factors below 35%, the difference is positive, i.e. the relative resistance computed from the model is greater than that computed by the FEM. The variation between the two methods is due to the definition of the limits of the perturbed zone. Inversely, at high covering factor, the relative resistance calculated from the model

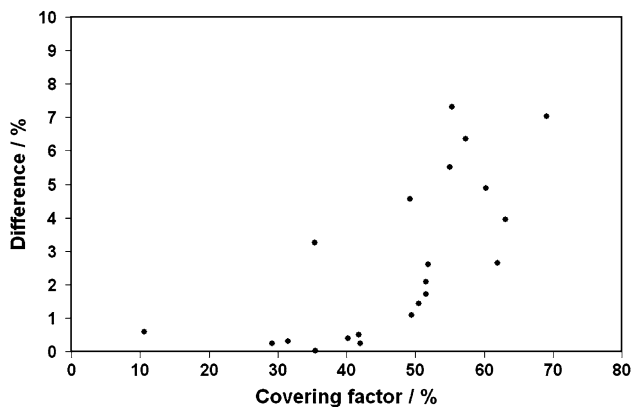


Fig. 8. Difference between the relative resistance calculated from the proposed model and the FEM versus the covering factor.

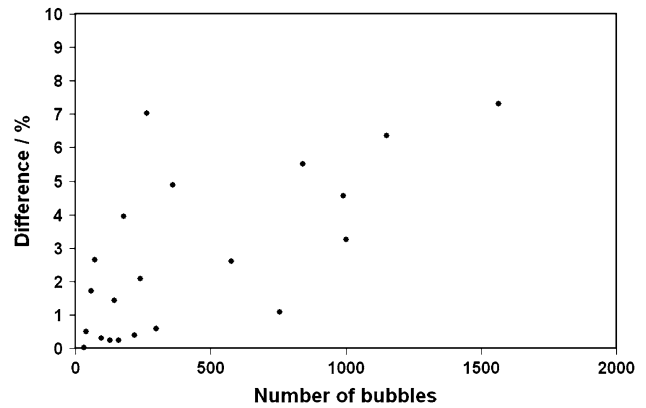


Fig. 9. Difference between the relative resistance calculated from the proposed model and the FEM versus the number of bubbles.

is smaller than that obtained from the FEM. The discrepancy is due to the fact that the model does not take into account the increment of the resistance caused by the introduction of a non-linearity in the domain of solutions.

In this section, the model has been validated for many bubble size distributions as well as for several covering factors. It gives good agreement with the finite element method.

5. Conclusion

In this paper a model has been developed to compute the electrical resistance of the electrolyte in the presence of bubbles using the concept of parallel connected current tubes associated with the individual bubbles. The proposed model is computationally more efficient than the numerical solution of the Laplace equation for the two-phase layer with a large number of bubbles with different size and shape, as it uses the solutions obtained earlier for the individual current tubes as a function of the size and shape of bubbles. The screening effect as well as the deformation of the

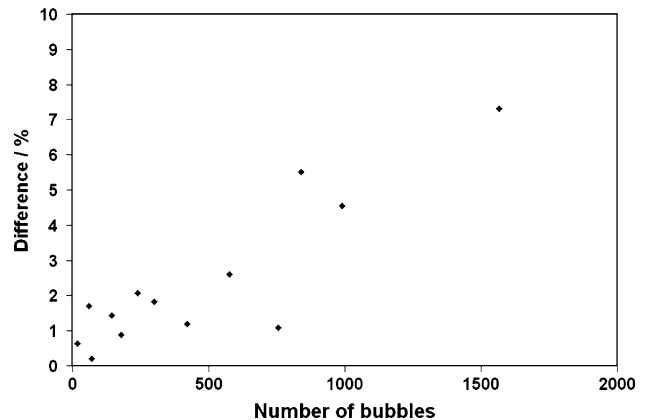


Fig. 10. Difference between the relative resistance calculated from the proposed model and the FEM versus the number of bubbles at a covering factor of around 50%.

electrical field caused by the presence of bubbles is taken into account in this model. The model has been validated in several situations and it gives good agreement compared to the solutions obtained by a finite element method FEM for a large number of bubbles. Under normal operating conditions, the discrepancy between the proposed model and the FEM is around 5%. The aim of this project is to obtain a correlation between the electrical resistance of the electrolyte and the industrial parameters such as the current density, anode geometry and chemical composition of the bath. In order to calculate the overall electrical resistance by the method proposed in the present paper, the knowledge of the size, shape and position of all the bubbles is required as input of the model. These data can be obtained as time series computed by a numerical method like for example the bubble simulator developed by Kiss et al. [14–16]

Acknowledgements

The first author gratefully acknowledges the support of the Fonds québécois de recherches sur la nature et les technologies (FQRNT) and that of the Conseil de Recherches en Sciences Naturelles et en Génie du Canada (CRSNG) in the form of post-graduate scholarships.

References

1. K. Grjotheim and H. Kvande (eds), *Introduction to Aluminium Electrolysis*, 2nd edn., (Aluminium-Verlag, 1993).
2. W.E. Haupin, *J. Metals* **23** (1971) 46.
3. H. Vogt, *J. Appl. Electrochem.* **13** (1983) 87.
4. A. Solheim and J. Thonstad. in R.B. Miller and W.S. Peterson (eds.), *Light Metals*, (TMS, Warrendale, PA, 1986), pp. 397–403.
5. J. Zoric and A. Solheim, *J. Appl. Electrochem.* **30** (2000) 787.
6. J. Thonstad, H.D. Kleinschrodt and H. Vogt. in A.T. Tabereaux (ed.), *Light Metals*, (TMS, Warrendale, PA, 2004), pp. 427–432.
7. R.C. Dorward, *J. Appl. Electrochem.* **13** (1983) 569.
8. T.M. Hyde and B.J. Welch. in R. Huglen (ed.), *Light Metals*, (TMS, Warrendale, PA, 1997), pp. 333–340.
9. R.J. Aaberg, V. Ranum, K. Williamson and B.J. Welch. in R. Huglen (ed.), *Light Metals*, (TMS, Warrendale, PA, 1997), pp. 341–346.
10. K. Quian, J.J.J. Chen and N.J. Matheou, *J. Appl. Electrochem.* **27** (1997) 434.
11. K. Quian, D. Chen and J.J.J. Chen, *J. Appl. Electrochem.* **28** (1998) 1141.
12. D. Kasherman and M. Skyllas-Kazacos, *J. Appl. Electrochem.* **21** (1991) 716.
13. D.A.G. Bruggeman, *Ann. Phys.* **24** (1935) 636.
14. L.I. Kiss and S. Poncsák. in W. Schneider (ed.), *Light Metals*, (TMS, Warrendale, PA, 2002), pp. 217–223.
15. L.I. Kiss, S. Poncsák and J. Antille. in H. Kvande (ed.), *Light Metals*, (TMS, Warrendale, PA, 2005), pp. 559–564.
16. S. Poncsák, L.I. Kiss, D. Toulouse, A.L. Perron and S. Perron. in T.J. Galloway (ed.), *Light Metals*, (TMS, Warrendale, PA, 2006), pp. 557–562.
17. J.M. Purdie, M. Bilek, M.P. Taylor, W.D. Zhang, B.J. Welch and J.J.J. Chen. in S.K. Das (ed.), *Light Metals*, (TMS, Warrendale, PA, 1993), pp. 355–360.
18. T. Haarberg, A. Solheim, S.T. Johansen and P.A. Solli. in B.J. Welch (ed.), *Light Metals*, (TMS, Warrendale, PA, 1998), pp. 475–481.
19. K. Bech, S. Johansen, A. Solheim and T. Haarberg. in J.L. Anjier (ed.), *Light Metals*, (TMS, Warrendale, PA, 2001), pp. 463–468.
20. C. Kleinstreuer, *Two-Phase Flow Theory and Applications*, (Taylor and Francis Books Inc., 2004).
21. A.L. Perron, Rôle de la couche gazeuse dans les phénomènes de transport se produisant à l'intérieur d'une cuve Hall-Héroult, Ph.D Thesis, (Université du Québec à Chicoutimi, Canada, 2006).
22. A.L. Perron, L.I. Kiss and S. Poncsák, *J. Appl. Electrochem.* (in Press).
23. S. Fortin, M. Gerhardt and A.J. Gesing. in J.P. McGeer (ed.), *Light Metals*, (TMS, Warrendale, PA, 1984), pp. 721–741.